EC Journals.ASM.org

Active Hydrocarbon Biosynthesis and Accumulation in a Green Alga, *Botryococcus braunii* (Race A)

Mana Hirose,[a] Fukiko Mukaida,[a] Sigeru Okada,[b,c] Tetsuko Noguchi[a,c]

Department of Biological Sciences, Nara Women's University, Nara, Japan[a]; Department of Aquatic Biosciences, The University of Tokyo, Bunkyo, Tokyo, Japan[b]; JST, CREST, Chiyoda, Tokyo, Japan[c]

Among oleaginous microalgae, the colonial green alga *Botryococcus braunii* accumulates especially large quantities of hydrocarbons. This accumulation may be achieved more by storage of lipids in the extracellular space rather than in the cytoplasm, as is the case for all other examined oleaginous microalgae. The stage of hydrocarbon synthesis during the cell cycle was determined by autoradiography. The cell cycle of *B. braunii* race A was synchronized by aminouracil treatment, and cells were taken at various stages in the cell cycle and cultured in a medium containing [^{14}C]acetate. Incorporation of ^{14}C into hydrocarbons was detected. The highest labeling occurred just after septum formation, when it was about 2.6 times the rate during interphase. Fluorescent and electron microscopy revealed that new lipid accumulation on the cell surface occurred during at least two different growth stages and sites of cells. Lipid bodies in the cytoplasm were not prominent in interphase cells. These lipid bodies then increased in number, size, and inclusions, reaching maximum values just before the first lipid accumulation on the cell surface at the cell apex. Most of them disappeared from the cytoplasm concomitant with the second new accumulation at the basolateral region, where extracellular lipids continuously accumulated. The rough endoplasmic reticulum near the plasma membrane is prominent in *B. braunii*, and the endoplasmic reticulum was often in contact with both a chloroplast and lipid bodies in cells with increasing numbers of lipid bodies. We discuss the transport pathway of precursors of extracellular hydrocarbons in race A.

The fact that oxygenic photosynthetic microorganisms have the ability to produce substantial amounts of lipids has attracted attention with respect to production of renewable biofuels. During the past few decades, many algal and cyanobacterial species have been screened for high lipid content, and some green algae, diatoms, *Euglena*, and cyanobacteria have been characterized as oleaginous and examined for potential use in an alga-based biofuel industry (1, 2). In fact, such organisms could potentially produce 8 to 24 times more biofuel per unit area than the best land plants (3).

Among oleaginous microalgae, the colonial green alga *Botryococcus braunii* accumulates especially large quantities of hydrocarbons; the best record was 86% of its dry weight for an algal sample harvested from a natural bloom (4–7). This accumulation seems to be achieved by storage of most of the lipids in the extracellular space (8–11). In contrast, all other examined microalgae store lipid bodies in the cytoplasm. *B. barunii* is classified into three principal races, A, B, and L, depending on the types of hydrocarbons synthesized (12, 13). Race A produces alkadienes and alkatrienes (14), race B produces mainly triterpenoids known as botrococcenes (15, 16), and race L produces a tetraterpenoid known as lycopadiene (17). In both races A and B, the biosynthetic pathways to these hydrocarbons have been clarified, and some of the enzymes involved in the synthetic activity have been characterized (18–24). In addition, the associated patterns of gene expression have been examined to clarify the biosynthetic pathways to hydrocarbons (25–27).

Given the increase of physiological, molecular, and genetic information about hydrocarbon synthesis in *B. braunii*, further understanding of this process also requires basic cytological information. The high rates of hydrocarbon production by *B. braunii* had already attracted the attention of phycologists more than 30 years ago, and interesting cytological experiments were carried out with techniques such as chemical analysis of hydrocabons, radiolabeling, and electron microscopy. However, the major ultrastructural studies with electron microscopy were limited to the period from 1978 to 1984 (6, 8, 28, 29). In the case of *B. braunii*, the use of conventional chemical fixation for electron microscopy failed to show the fine ultrastructure of the cells, especially the cytoplasm, probably because the large amount of lipid that accumulated around cell surfaces interfered with the penetration of fixatives and embedding resin. We overcame this weakness by using a rapid freezing and freeze-substitution method for electron microscopic analysis and were thus able to advance studies of the transformation of *trans*-Golgi networks throughout the cell cycle of race A (30–32). Recently, Weiss et al. examined the extracellular matrix and intercellular structures of *B. braunii* race B by another rapid-freezing method—quick-freeze deep-etch electron microscopy—and clarified its colony organization (33).

The goals of this study were to (i) determine the stage(s) of the cell cycle during which hydrocarbon synthesis occurs, (ii) analyze the behavior and structural changes of lipid bodies during the cell cycle, (iii) clarify the stage and site of extracellular hydrocarbon accumulation during the cell cycle, and (iv) based on the results of goals i to iii, discuss the transport pathway of the precursors of extracellular hydrocarbons.

Received 5 April 2013 Accepted 16 June 2013
Published ahead of print 21 June 2013
Address correspondence to Tetsuko Noguchi, noguchi@cc.nara-wu.ac.jp.
Supplemental material for this article may be found at http://dx.doi.org/10.1128/EC.00088-13.

doi:10.1128/EC.00088-13

Although a method for synchronous culture of *B. braunii* had not been established, synchronous growth was essential for the first experimental purpose (goal i). Until now, we have succeeded in synchronizing the growth of only race A. We therefore selected race A for this experimental study. The alkadienes and alkatrienes synthesized by race A are straight, odd-number C_{27}, C_{29}, and C_{31} hydrocarbon chains, each of which has two or three double bonds (12). These chains are produced by elongation of oleic acid (C_{18}) followed by loss of the carboxyl carbon (18, 19). Various growth conditions have been examined to maximize hydrocarbon production, and it has been reported that hydrocarbons are produced mainly during the exponential and linear phases of culture growth (7, 13). These results indicate that active hydrocarbon synthesis accompanies cell division. However, the exact phase of the cell cycle associated with hydrocarbon synthesis has not been clarified. Because [1-^{14}C]acetate is readily incorporated into hydrocarbons of race A (18), the rate of synthesis of hydrocarbons at different stages of the cell cycle can be estimated from the incorporation of [^{14}C]acetate into hydrocarbons. Our ability to synchronize the growth of race A allowed us to obtain unambiguous results.

Lipid accumulation in the extracellular space in *B. braunii* is the major factor that distinguishes it from other oleaginous microalgae. The major lipid components produced by *B. braunii* are hydrocarbons, and most of them accumulate in the extracellular space; 90 to 95% external compared to 10 to 5% internal in experiments with race A (7–9). Until now, an idea proposed in 1980 by Largeau et al. (9) has been cited in papers, namely, that hydrocarbon secretion does not occur in race A of *B. braunii*, and there has been no information about the transport pathway of hydrocarbon precursors in the cytoplasm. Because the precursors must be transported from sites of synthesis in the cytoplasm to the cell surface as hydrocarbon synthesis progresses, their transport pathway has remained a focus of research. This study shows that new lipid accumulation occurs at the cell apex and at the basolateral region, the latter being the site of most accumulation in race A; the transport pathway of precursors of extracellular hydrocarbons is discussed based on the distribution of the endoplasmic reticulum (ER) and the behavior of lipid bodies that occur concomitant with new lipid accumulation on the cell surface.

MATERIALS AND METHODS

Strains and culture conditions. *Botryococcus braunii* Kützing (UTEX 2441) was obtained from the Culture Collection of Algae at the University of Texas at Austin; *B. braunii* Kützing (807/1, Droop, Maddingley, Brick Pits, United Kingdom) from the Göttingen Culture Collection (Germany).

Cells were cultured in Chu10 medium at 22°C. They were illuminated for 13 h per day with fluorescent light at a photon flux density of 50 μmol·m^{-2}· s^{-1}. To induce synchronized cell division, we used 0.5 mM aminouracil (Nacalai Tesque, Inc., Kyoto, Japan) to block the cell cycle in the S phase. Aminouracil was dissolved at a concentration of 2.5 mM in distilled water, which was then autoclaved at 110°C for 10 min (stock solution). The sterile aminouracil solution was then added to the culture medium. One-month-old cell cultures (UTEX 2441) were transferred to a new culture medium 1 h before illumination to induce cell division. They were allowed to grow until 1 h before the next dark period (i.e., for 13 h), treated with 0.5 mM aminouracil for another 24 h, washed with aminouracil-free culture medium 6 times for a total of 1 h, and then transferred to fresh medium.

Incorporation of [1-^{14}C]acetate into hydrocarbons. Synchronously growing cells (UTEX 2441) under the same culture conditions were harvested 5, 13, 21, and 48 h after the aminouracil was washed out. The cells were placed in 10-ml test tubes containing 2.5 μCi sodium [1-^{14}C]acetate and 5 ml of culture medium. The test tubes were shaken on a reciprocal shaker at 60 cycles min^{-1} in darkness at 22°C for 2 h. Radiolabeled cells were washed with ^{14}C-free culture medium, boiled for 1 min to stop hydrocarbon synthesis, washed 8 times with distilled water, and dried in a micropetri dish.

Lipids were extracted from 10 mg of each dried sample at room temperature with *n*-hexane for 4 h (two times for 2 h each) and then with chloroform-methanol (2:1 vol/vol) for 24 h, in both cases with efficient stirring. All extracts were combined, and the solvents were evaporated. The lipids were separated by thin-layer chromatography (TLC) on Whatman silica gel 60-Å plates with *n*-hexane–diethyl ether–formic acid (40:10:1 vol/vol/vol) as the chromatography solvent. The radioactive bands (R_f, 0.93) were located by autoradiography with Fuji medical X-ray film. The intensities of the autoradiographic images of the hydrocarbon bands were measured with a densitometer.

Analysis of hydrocarbons. Cells were collected by centrifugation and dried in a micropetri dish. Lipids were extracted at room temperature from the dried samples by soaking in acetone. An acetone extract was obtained as a supernatant after centrifugation at 600 × *g* for 10 min at room temperature. This operation was repeated until the supernatant became colorless. The acetone extracts were combined, evaporated, dissolved in *n*-hexane, and subjected to silica gel column chromatography using Wako gel C-300 as the stationary phase. A hydrocarbon fraction was obtained by elution with *n*-hexane. Hydrocarbon composition was determined by gas chromatography-mass spectrometry (GC-MS) with a Shimadzu GCMS-QP2010 Ultra equipped with a capillary column (InertCap 1MS, GL Science; 60 m by 0.25 m, film thickness, 0.25 μm). The column temperature was programmed as follows: 50°C for 1 min, increased at 10°C/min to 220°C and at 2°C/min to 260°C, and held for 50 min. The ion source and injection port were held at 200 and 260°C, respectively. Relative abundances of major components were calculated from their peak areas in the total ion chromatogram.

Light and fluorescence microscopy. Neutral red was dissolved in the culture medium at a concentration of 0.05%. Living cells were soaked in the staining solution for 20 min and were observed under a conventional light microscope.

For double staining with Nile red and neutral red, live cells were soaked in neutral red solution for 20 min. Then 1/200 volume of 1 mM Nile red solution (stock solution dissolved in dimethyl sulfoxide [DMSO]) was added, and the cells were stained for another 4 min. The cells were then washed four times with culture medium, mounted on a slide glass, and slightly pressed with a coverslip to obtain most of the lipid bodies/vacuoles in a focal plane and observed by using light (neutral red) and fluorescence (Nile red) microscopy.

Electron microscopy. Algal cells of the Göttingen strain at different developmental stages were attached to Formvar films mounted on copper wire loops 8 mm in diameter and were frozen in liquid propane at −190°C. They were then transferred to acetone (−85°C) that contained 2% osmium tetroxide and 0.2% uranyl acetate. After 48 h at −85°C, the samples were gradually warmed to room temperature, washed with acetone, and embedded in Spurr resin. Sections were stained with lead citrate and examined in a Hitachi H-7000 or JEM-1230 transmission electron microscope or an ultra-high-voltage electron microscope.

RESULTS

Cell growth and hydrocarbon synthesis during the cell cycle. Analysis of the hydrocarbons synthesized by the UTEX 2441 strain under our culture conditions showed that $C_{27}H_{52}$, $C_{29}H_{56}$, and $C_{31}H_{60}$ alkadienes were the main products and accounted for 20.8%, 35.8%, and 14.4% of the total hydrocarbons, respectively (Table 1). No alkatrienes were detectable, whereas small amounts of C_{23}, C_{25}, C_{27}, C_{29}, and C_{31} monoenes were present in this strain. The composition of hydrocarbons produced by the Göttingen strain (see Table S1 in the supplemental material) suggested that,

TABLE 1 Composition of the hydrocarbons from *B. braunii* race A (UTEX 2441)

Hydrocarbon	Mol wt	%
$C_{23}H_{44\alpha}$	320	0.1
$C_{23}H_{44\beta}$	320	0.4
$C_{23}H_{46}$	322	0.7
$C_{25}H_{48\alpha}$	348	0.8
$C_{25}H_{48\beta}$	348	3.2
$C_{25}H_{50}$	350	0.7
$C_{27}H_{52\alpha}$	376	11.1
$C_{27}H_{52\beta}$	376	9.7
$C_{27}H_{54}$	378	3.7
$C_{29}H_{56}$	404	35.8
$C_{29}H_{58}$	406	9.4
$C_{31}H_{60}$	432	14.4
$C_{31}H_{62}$	434	1.0
$C_{33}H_{64}$	460	1.2
Unidentified		7.8

like the UTEX 2441 strain, it is a typical strain of race A. For measurements of hydrocarbon synthesis, we used UTEX 2441 because it is axenic.

We made our cell cultures grow synchronously by treating them with aminouracil (Fig. 1). The percentage of synchronization was about 80% (i.e., the ratio of synchronously growing cells to interphase cells was about 4:1). Five hours after removal of the aminouracil (4 h after the beginning of the dark period), the cells were swollen (Fig. 1A2) compared to interphase cells (Fig. 1A1), but there was no septum visible in any cell, the indication being that cell division had not yet begun. The volumes of the cells 13 h and 5 h after removal of the aminouracil were the same, but at 13 h a fine septum was visible across the center of each cell (Fig. 1A3). After 21 h, a pair of daughter cells (autospores) was clearly seen inside the mother cell wall (Fig. 1A4). After 48 h, cells were no longer paired and were liberated from the mother cell wall (Fig. 1A5).

The cells shown in Fig. 1 were treated with neutral red. Particles 1 to 2 μm in diameter around the nuclei of the interphase cells stained strongly (Fig. 1A1). It is well known that neutral red selectively enters the vacuoles in plant cells. Red particles were therefore identified as vacuoles. Particles that stained with neutral red were rare in dividing cells (Fig. 1A3 and A4) (for details, see reference 30). Forty-eight hours after removal of aminouracil (Fig. 1A5), the vacuoles of cells heavily stained with neutral red again appeared, the indication being that the 48-h cells may have been physiologically the same as interphase cells.

The *B. braunii* cells grew very slowly in synchronized cultures. About 16 h elapsed from the beginning of cell growth (Fig. 1A2) to the formation of autospores (Fig. 1A4). This transition seemed to take less time in untreated cultures, in which growing cells just after cell division were prominent 5 h after the beginning of the dark period. We could not observe the real time required for growth, because *B. brauniii* is a very sensitive alga, and the growth stage of growing cells did not progress under a light microscope, although we have made analogous light microscopic observations successfully with many other algae.

The stage of hydrocarbon synthesis during the cell cycle was determined by incorporation of radiolabeled [^{14}C]acetate into hydrocarbons produced in synchronized cell cultures at various stages. Figure 1B shows the results of two experiments, one (dark bars) of which was carried out with the cell cultures shown in Fig. 1A2 to A5. The ^{14}C labeling of hydrocarbons in cells occurred throughout the cell cycle. The highest ^{14}C labeling occurred just after septum formation (corresponding to Fig. 1A3), when the amount of ^{14}C-labeled hydrocarbons was more than 250% that of

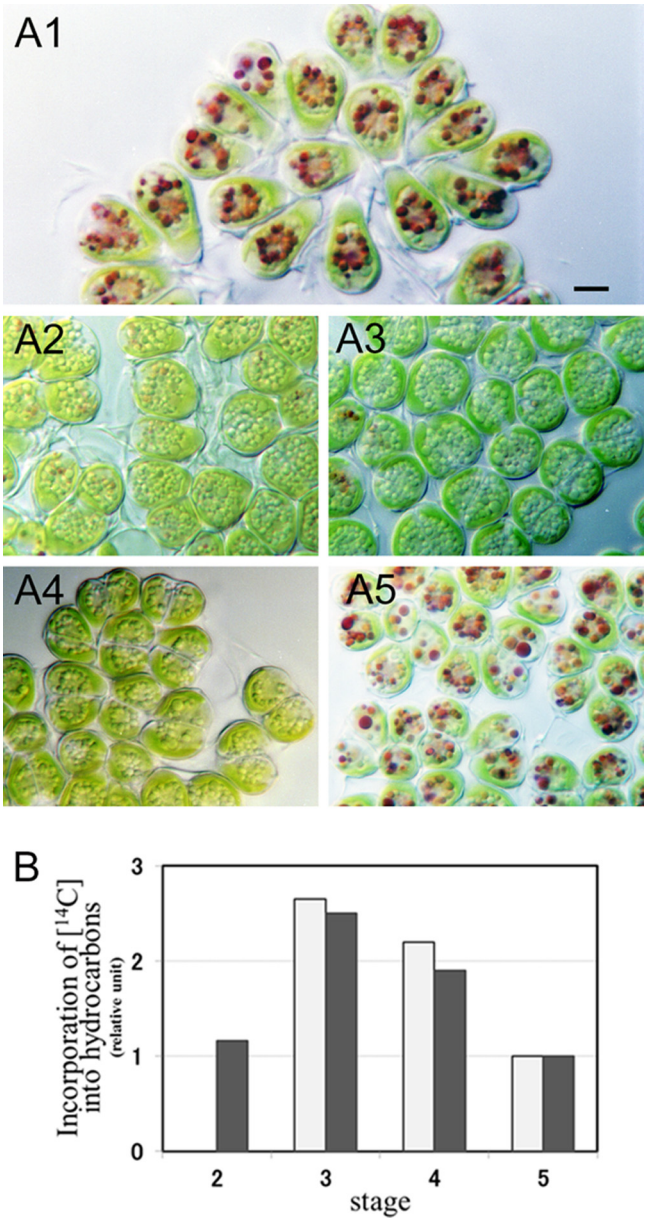

FIG 1 Hydrocarbon synthesis during the cell cycle. (A) Synchronously growing *B. braunii*. (A1) Interphase cells; (A2) cells just before cell division (5 h after removal of aminouracil); (A3) cells just after septum formation (13 h); (A4) a pair of daughter cells within the mother cell wall (21 h); (A5) interphase cells (48 h). All cells were treated with neutral red. Size bar, 5 μm. (B) Incorporation of ^{14}C into hydrocarbons. Cells were cultured in a medium containing 2.5 μCi sodium [1-^{14}C]acetate for 2 h, and the incorporation of ^{14}C into hydrocarbons was measured. Experiments were carried out twice (dark and white bars), except for stage 2. The dark bar shows the results of an experiment with the cells shown in Fig. A2 to 5. Stage 2, just before cell division (corresponds to panel A2); stage 3, just after cell division (A3); stage 4, stage of a pair of daughter cells within a mother cell wall (A4); stage 5, interphase (A5).

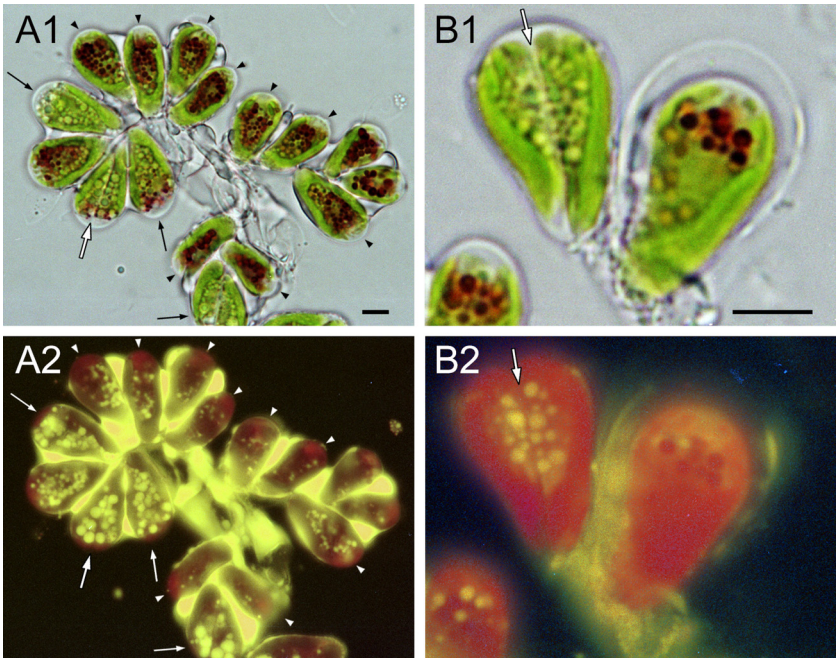

FIG 2 Cells double stained with Nile red and neutral red. (A1 and B1) Neutral red, light microscopy. (A2 and B2) Nile red, fluorescence microscopy. (A) A colony with cells at three different stages. In stage 1, interphase cells (arrowheads) have many neutral-red-positive particles localized around the cell center. These cells also contain smaller particles faintly stained with Nile red. In stage 2, growing cells (thin arrows), which we assume are preparing to enter or are just entering mitosis, are also particle rich. Differently from interphase cells, most particles are intensely stained with Nile red. In stage 3, dividing cells with septum (A1, large open arrow; A2, large white arrow) also have many yellow particles that are larger than those in interphase cells. Size bar, 5 μm. (B) Enlargement of double-stained cells. In a cell just after septum formation (left), particles are strongly stained with Nile red but cannot be stained with neutral red. White arrow; septum. Size bar, 5 μm.

interphase cells (Fig. 1A5). The same radiolabeling experiment was done five times with interphase cells that were not treated with aminouracil, and a substantial amount of [^{14}C]acetate was incorporated into hydrocarbons in all experiments (data not shown).

Behavior of the lipid body and vacuole. When 1-month-old cell cultures were transferred into a new culture medium 1 h before illumination, about 20% of the cells started to divide in the dark period after 2 days. Colonies from the culture were double stained with the fluorescent lipophilic dye Nile red and neutral red to clarify the relative behavior of the lipid body and the vacuole (Fig. 2). *B. braunii* formed amorphous, three-dimensional microcolonies, wherein individual cells were held together at the bottom by a matrix stained by Nile red (Fig. 2A2, yellow). Because hydrocarbons accounted for the major part of total lipids in most strains of *B. braunii*, we assumed that the main component in the matrix consisted of hydrocarbons. A cup-shaped chloroplast occupied the cell bottom. In interphase cells, many vacuoles were present in the center of cells (Fig. 2A1; black arrowheads; see Fig. S1B, stage 1, in the supplemental material), but lipid bodies were small and not prominent (Fig. 2A2, white arrowhead; see Fig. S1A, stage 1). When cells entered the M phase (mitosis and cytokinesis), lipid bodies increased in number and size (Fig. 2A, thin arrows; see Fig.S1A, stage 2). In cells with a clear septum (Fig. 2A1 and B, white arrows) that had lost vacuoles, large lipid bodies stained with Nile red were prominent (Fig. 2A2 and B1, left cell; see Fig. S1, stage 3).

Ultrastructure of a cell visualized by electron microscopy. The center of the cell was occupied by the nucleus, which was surrounded by vacuoles with tonoplasts (Fig. 3A and B). There was a cup-shaped chloroplast at the bottom of the cell, and the Golgi apparatus (6 to 8 Golgi bodies/cell) (32) was in the upper portion of the cell (cell apex). A layer having a uniform thickness completely surrounded the plasma membrane and was composed, inter alia, of cellulose, pectin, and hemicellulose (T. Noguchi, unpublished data). We have therefore characterized this layer as a polysaccharide cell wall in this article. Each cell was covered with amorphous materials and thin layers in the basolateral region; the former occupied 70 to 90% of the cell surface (Fig. 3A). These materials and layers might be extracellular lipids containing hydrocarbons, because they stained with Nile red (Fig. 2A2).

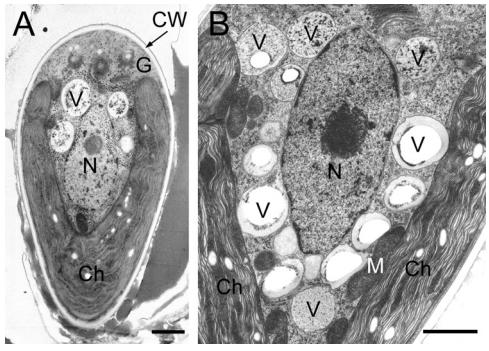

FIG 3 Electron microscopy of an interphase cell. (A) Longitudinal section of the cell. (B) Vacuoles around nucleus. Ch, chloroplast; CW, cell wall; G, Golgi body; M, mitochondria; N, nucleus; V, vacuole. Size bars, 1 μm.

Behavior of the lipid body and vacuole visualized by electron microscopy. ^{14}C incorporation into hydrocarbons was highest just after septum formation. In addition to vacuoles, we therefore focused on lipid bodies and the endoplasmic reticulum (ER) before and after septum formation and, as a control, during interphase. Particles without a unit membrane (lipid bilayer) were identified as lipid bodies, and a particle with a unit membrane was identified as a vacuole with a tonoplast, because the size, location within the cell, and behavior of the former were similar to those of lipid bodies stained with Nile red and of the latter to those of vacuoles stained with neutral red in Fig. 2. Both kinds of particles were always located in the space between a nucleus and a chloroplast. In cells at an early stage of cell growth before nuclear division (Fig. 4A), there were recently formed lipid bodies between the chloroplast and nucleus, more than half the contents of which consisted of electron-transparent regions. The lipid bodies were covered with the rough endoplasmic reticulum (rER), but the rER had lost ribosomes from the surface facing toward the lipid bodies (Fig. 4A, insert, arrowheads), and the vacuoles were also covered with rER. In growing cells before septum formation (Fig. 4B), lipid bodies were covered with electron-transparent belts, the outlines of which were wavy. The electron-transparent region within these lipid bodies was smaller; in other words, the volume of the electron-dense region had increased. Sometimes, the rER near the chloroplast envelope reached to the surface of lipid bodies and had lost ribosomes from the surface facing toward them (Fig. 4B, insert, arrowhead). The rER was also developed in the upper region of cells. In cells just after septum formation but before polysaccharide cell wall formation (Fig. 4C), there were few vacuoles, and we observed typical lipid bodies that lacked electron-transparent regions and had a clear outline expected for a lipid monolayer. In cells during the formation of a polysaccharide cell wall around daughter cells (Fig. 4D), Golgi bodies produced vesicles with an electron-dense core, and lipid bodies maintained a clear outline, but an electron-transparent region appeared again. After polysaccharide cell wall formation, the divided chloroplast recovered its volume and finally became cup shaped. In a pair of daughter cells recovering chloroplasts (Fig. 4E), lipid bodies remained in number and appearance similar to those in previous stages. In mature cells accumulating new lipid droplets between the new cell wall and a thin outer layer (Fig. 4F and G), lipid bodies had lower electron densities and were covered by a structure similar to smooth endoplasmic reticulum (sER), with a wavy outline (Fig. 4F), or disappeared (Fig. 4G). Vacuoles containing electron-dense amorphous materials appeared (Fig. 4F) and became prominent (Fig. 4G).

Stage and site of new extracellular lipid accumulation. Round lipid droplets on the cell surface were considered to be lipids recently secreted to the cell surface. They were observed during at least two special stages: just before (Fig. 5A) and after (Fig. 5B) septum formation and after polysaccharide cell wall formation in mature cells (Fig. 5C). In Fig. 5A, lipid droplets stained with Nile red are observed on and outside the cell apex (yellow ellipses). This phenomenon was very surprising, because hydrocarbons usually do not accumulate at the cell apex (Fig. 2, 3, 4, and 5C and D). We therefore confirmed the phenomenon by observing a 500-nm-thick section with ultra-high-voltage (2,000-kV) electron microscopy. Figure 5B is a longitudinal section of a cell in which a septum has already formed, and electron-dense droplets are prominent on the mother cell wall at the cell apex. Because this phenomenon was infrequently observed, it may occur during a short period of time.

Electron microscopy also revealed round lipid droplets in the basolateral region. In Fig. 5C, many round lipid droplets (brackets) can be seen attached to the cell surface where a recovered chloroplast is located nearby, and there is a thin layer with round lipid droplets and amorphous materials surrounding the whole cell (arrows). The extracellular thin layer with amorphous materials corresponded to the "trilaminar sheath" reported by Largeau et al. (8) and easily peeled off (Fig. 5D). We observed electron-transparent thin layers only in the amorphous materials (Fig. 5C and E), but not in round lipids recently secreted to the cell surface (Fig. 5C, brackets). New lipid accumulation in the basolateral region could not be detected by Nile red staining because the lipids were mixed with preexisting extracellular lipids, including hydrocarbons.

Cortical ER under the plasma membrane. The cortical ER was prominent in *B. braunii*. Because it was located in a similar position throughout the cell cycle, we therefore show the ER in a cell at an early stage of polysaccharide cell wall formation (Fig. 6), when lipid-like substances accumulated between septa (Fig. 6D) and in an interphase cell (see Fig. S2 in the supplemental material). It is generally accepted that a cell has one ER. Therefore, the cortical ER located near the plasma membrane shown in Fig. 6 is considered to be one fenestrated sheet, partially smooth and partially rough with attached ribosomes. The ER was located not only within the top of the cell (Fig. 6C) but also along with the septum (Fig. 6D) and in the narrow space between the chloroplast and the plasma membrane (Fig. 6B and E). The rER just under the plasma membrane often lacked ribosomes on the surface toward the plasma membrane (Fig. 6B, D, and E), and even the sER was observed in the basolateral regions (Fig. 6B and E).

DISCUSSION

We successfully observed recently accumulated extracellular lipids as spherical droplets on the cell surface (Fig. 5A to C). The accumulation of new lipid in the extracellular space (site and stage) and transformation of lipid bodies in the cytoplasm (location and inclusion) during the cell cycle are summarized in Fig. 7. Because the increase and decrease of vacuoles seem to be related to changes in the concentrations of lipids, their transformations have been added in Fig. 7. In interphase cells (stage 1), lipid bodies are small, and large vacuoles occupy the space between a nucleus and a chloroplast. When cells start to grow (stage 2), the sizes of the lipid bodies and their electron-dense inclusions gradually increase. Just after septum formation (stage 3), the lipid bodies reach a maximum in total volume per pair of daughter cells and are filled with electron-dense inclusions, and round lipid droplets appear on the cell surface at the cell apex. During polysaccharide cell wall formation (stage 4), lipid bodies retain their numbers, but electron-transparent regions appear in them. Accompanying recovery of the chloroplast in daughter cells (stage 5), vacuoles appear again. After recovery of the chloroplast (stage 6), round lipid droplets appear on the cell surface at the basolateral regions of cells, and lipid bodies disappear from the cytoplasm.

The increase and decrease of lipid bodies in the cytoplasm are inversely related to new lipid accumulation on the cell surface. In other words, there were small lipid bodies in interphase cells, the sizes of the lipid bodies and their inclusions then increased, and

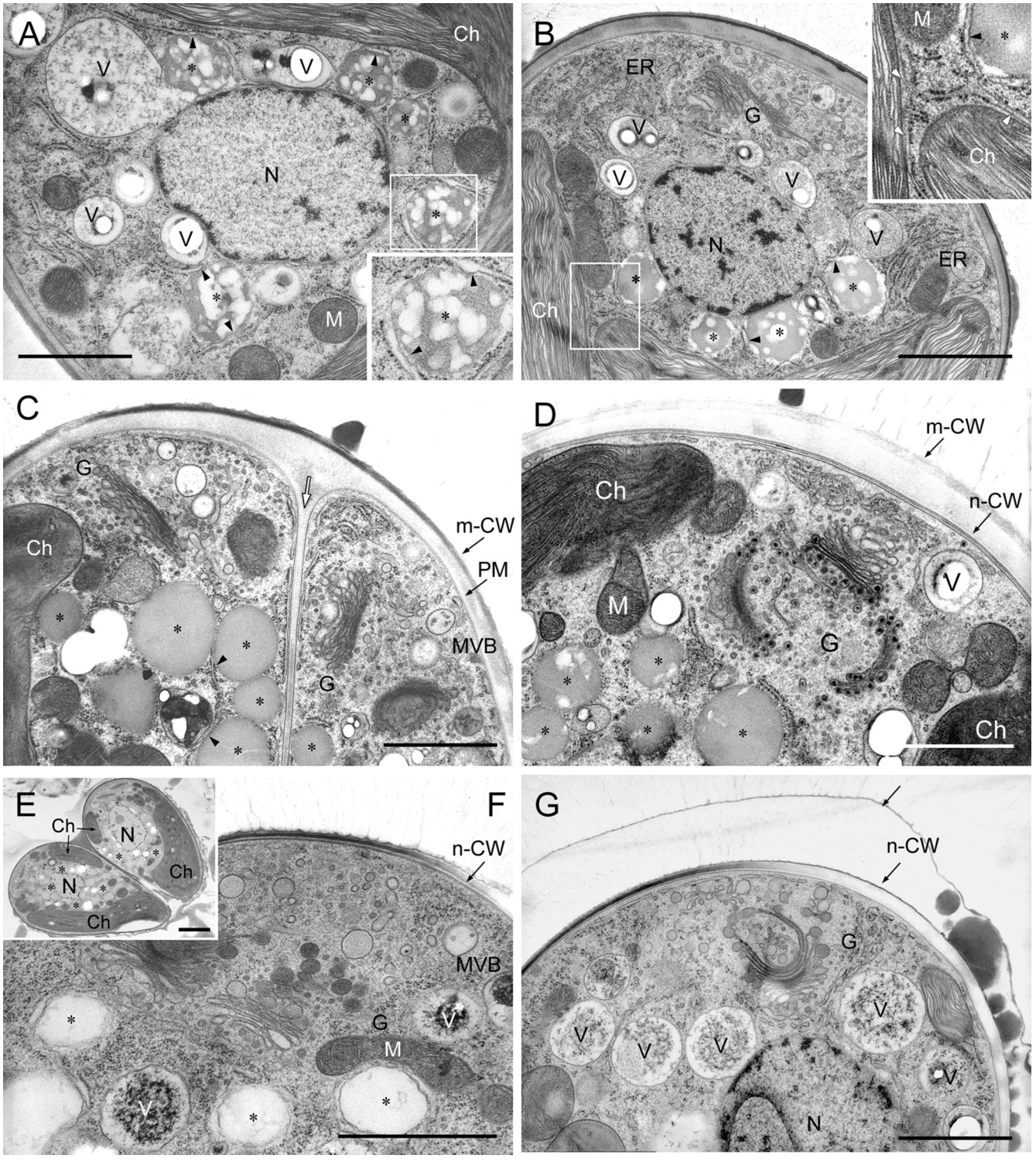

FIG 4 Morphological changes of lipid bodies and vacuoles in cells at different stages of growth. (A) Cell at an early stage of cell growth. The inset is an enlargement of the rectangle. (B) Cell just before septum formation. The inset is an enlargement of the rectangle. (C) Cell just after septum formation (white arrow) but before polysaccharide cell wall formation. (D) Cell during polysaccharide cell wall formation, in which Golgi bodies produce vesicles with an electron-dense core. (E) A pair of daughter cells recovering a chloroplast. Size bar, 2 μm. (F and G) Mature cell accumulating new lipids between its surface and a thin layer. Ch, chloroplast; ER, endoplasmic reticulum; G, Golgi body; m-CW, mother cell wall; N, nucleus; n-CW, new cell wall; PM, plasma membrane; V, vacuole; white arrow, septum; *, oil body; arrow, thin layer; arrowhead, ER lacking ribosomes from the surface facing toward the lipid body or the chloroplast. Size bars in panels A to D, F, and G, 1 μm.

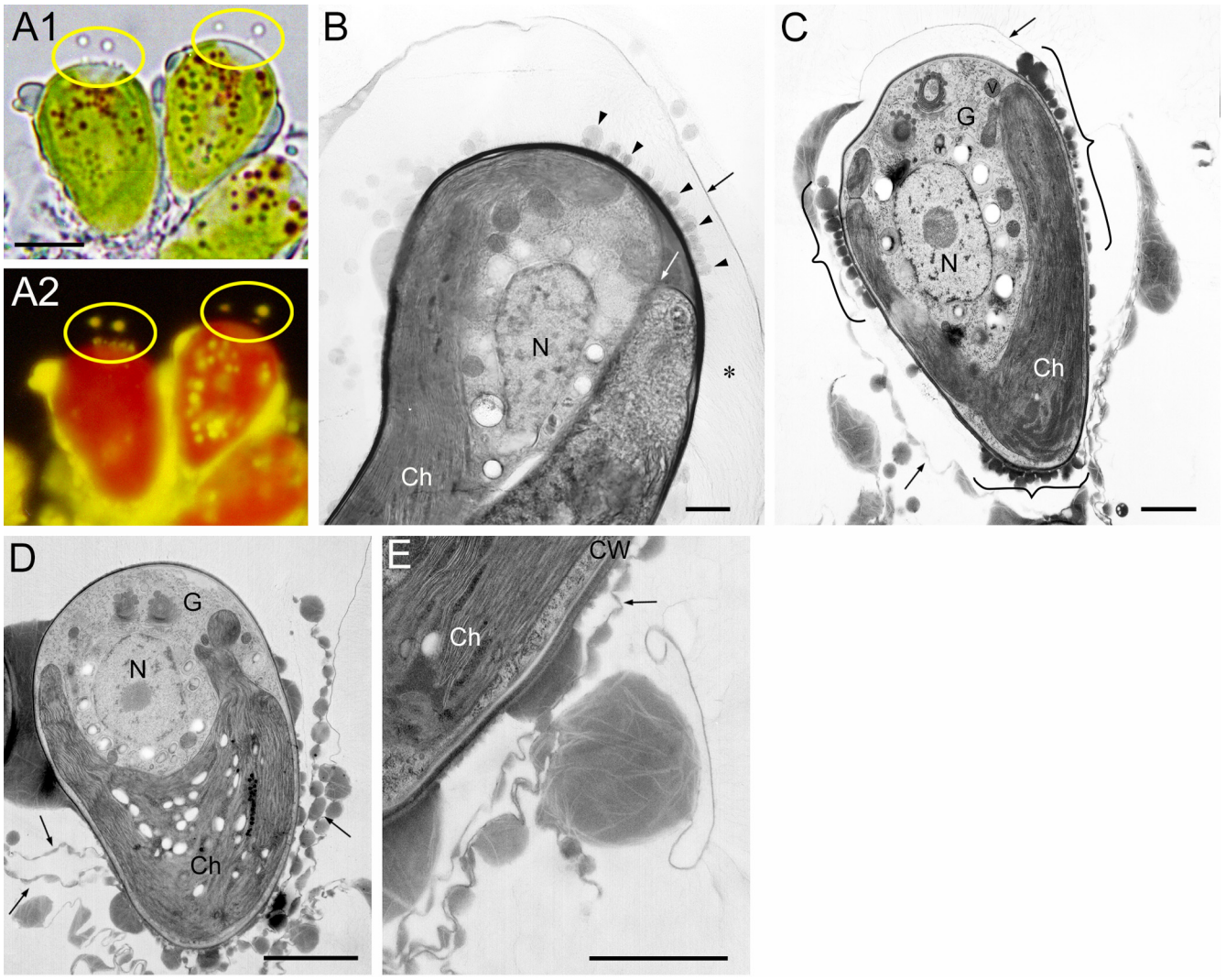

FIG 5 Recent accumulation of oil droplets on a cell surface and outer thin layer. (A) Cells at the growing stage before septum formation double stained with neutral red (A1) and Nile red (A2). Lipid droplets are seen on the surface of the cell apex (yellow ellipses). Size bar, 5 μm. (B) Cell just after septum (white arrow) formation in thick section (500 nm). Oil droplets (arrowhead) are seen on the cell wall at the cell apex. Fine fibrils (*) stretch from the cell wall to a thin layer separated from the cell wall. (C) Mature cell covered with a thin layer. Oil droplets (bracket) are seen on the new cell wall in the basolateral region. (D) Mature cell peeling off a thin layer from the cell apex. (E) Same stage as panel D. Amorphous materials are attached to thin layers, including electron-transparent layers. Ch, chloroplast; CW, cell wall; G, Golgi body; N, nucleus; black arrow, thin layer with amorphous material. Size bars in panels B to E, 1 μm.

both reached maximum values just before the first new accumulation of lipid at the cell apex. Most of the lipid disappeared from the cytoplasm concomitant with the second new accumulation of lipid in the basolateral region, where extracellular lipids were always observed. These results indicate that lipid bodies participate in the accumulation of extracellular lipid in *B. braunii* race A. The finding by Weiss et al. in 2010 that botryococcene, the major hydrocarbon of race B, was detected in cytoplasmic lipid bodies of race B by Raman spectroscopy (34) also supports the participation of lipid bodies in the accumulation of extracellular lipid.

Stage of active hydrocarbon synthesis during the cell cycle. Three main results of this study indicate that hydrocarbon synthesis occurs most actively just after septum formation. First, the highest rate of ^{14}C incorporation into hydrocarbons occurred just after septum formation. Second, Nile red staining showed that there were only a few, small lipid bodies in interphase cells; these increased in volume and number at the stage of cell growth, prior to active hydrocarbon synthesis. Third, supporting data from electron microscopy revealed that lipid bodies were completely filled with inclusions just after septum formation, in contrast to other stages of growth. The fact that a culture of race A increased in total hydrocarbon content in proportion to its total weight (7, 35) might reflect active hydrocarbon synthesis accompanying cell division.

At the same time, it also seems that hydrocarbon synthesis occurs throughout the cell cycle. Incubation with sodium [1-^{14}C]acetate showed that ^{14}C was incorporated into hydrocarbons not only just after cell division but also at other stages of the cell cycle (Fig. 1B). The control experiment showed that hydrocarbon synthesis does occur in interphase cells. In addition, all radiolabeling experiments on race A of *B. braunii* reported up to now have been carried out with nonsyn-

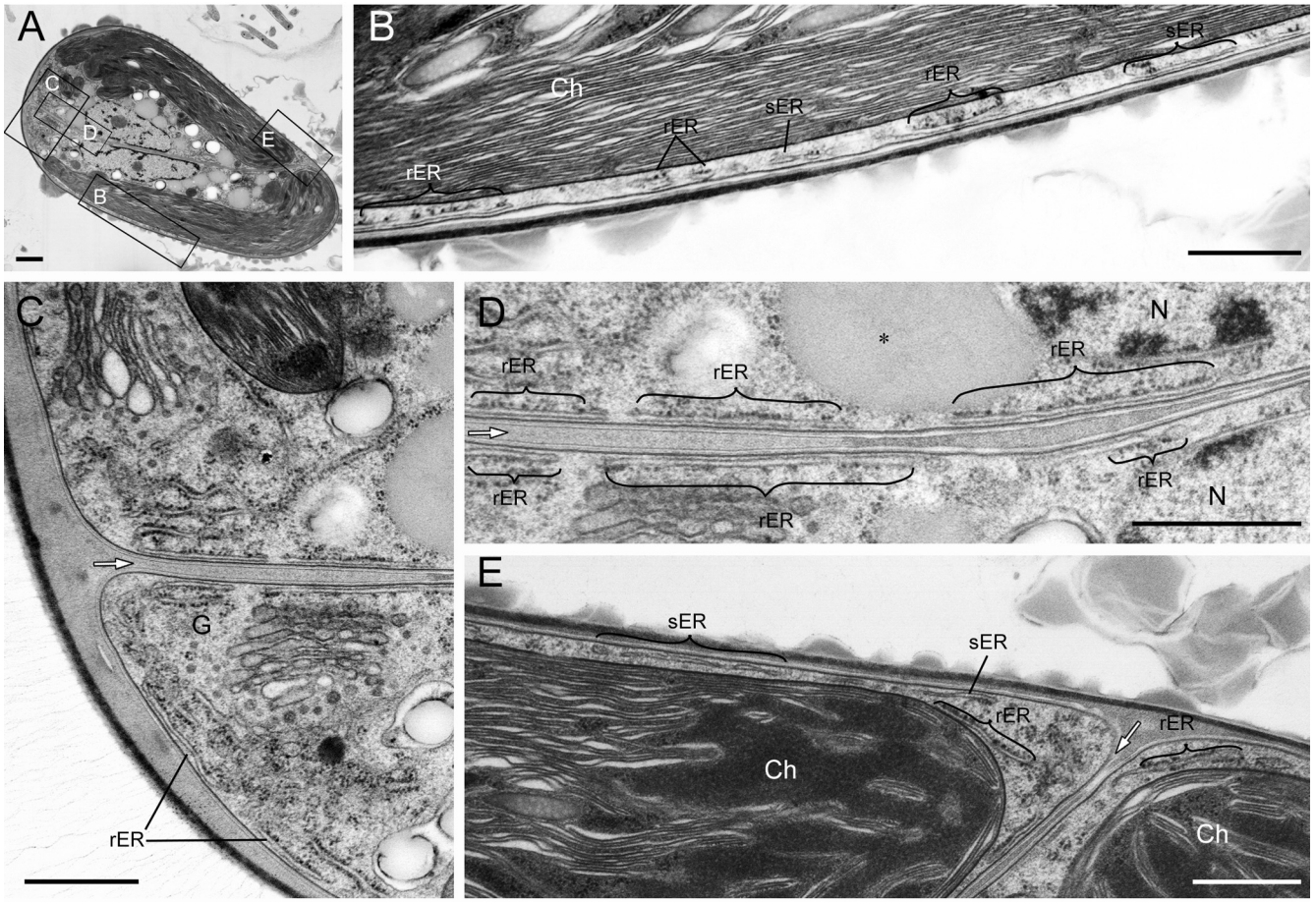

FIG 6 Cortical ER observed on thin section. (A) Low magnification. The rectangles labeled B, C, D, and E were enlarged to create panels B (lateral region), C (top region), D (septum region), and E (bottom region). The developed rER is prominent in the top region, and in the basolateral region the rER and sER are located between the plasma membrane and a chloroplast. The rER just under the plasma membrane lacks ribosomes on the surface facing the plasma membrane. Ch, chloroplast; G, Golgi body; white arrow, septum. Size bars, 1 μm in panel A and 0.5 μm in panels B to E.

chronized cultures, and the precursors, radiolabeled [^{14}C]acetate, [^{14}C]oleic acid, or [^{3}H]palmitic acid, have been incorporated into hydrocarbons within just 1 day and within as short a time as 1.5 h (9, 15, 35). In this context, a decarbonylase that catalyzes *n*-alkane production from fatty aldehydes was purified from a 10-day-old race A culture (19) in which the proportion of cells in the stage just after cell division would not be expected to be high.

Extracellular lipid accumulation and its transport pathway. Hydrocarbons are major lipid components produced by *B. braunii*, and most of them accumulate in the extracellular space. Lipid secretion is also an unusual phenomenon in higher plants, having been studied in epidermal cells covered by cuticular wax (36, 37) and the root cells of *Lithospermum erythrorhizon* accumulating shikonin (38). Among these three cases, biosynthesis of cuticular wax has been examined most thoroughly. Its biosynthesis begins with fatty acid synthesis (up to C_{18}) in the plastid. These fatty acids, elongated within the ER, are transferred to the plasma membrane from the ER or via Golgi bodies and are then secreted to the cell surface (36, 37). Shikonin (a naphthoquinone) or its precursor that is considered to be accumulated in the ER is transported to the plasma membrane by vesicles and secreted to the cell surface (38). In *B. braunii*, there has been no information about the transport pathway of hydrocarbon precursors in the cytoplasm. In this study, we clarified that the accumulation of new lipid at the basolateral region (stage 6 in Fig. 7) corresponded to a major site of lipid accumulation in race A. Because the alkadienes and alkatrienes produced by *B. braunii* race A are derived from fatty acid elongation in a manner similar to cuticular waxes, the initial steps of the biosynthetic pathway for them are considered to occur in the plastids (36, 37). The rER is often in contact with both a chloroplast and lipid bodies in cells with increasing numbers of lipid bodies (Fig. 4A and B, insets). In addition, the rER lost ribosomes from the surface facing the chloroplast or lipid bodies. A similar loss of rER ribosomes occurs at a budding site to form transport vesicles containing cargo proteins that are transported to the Golgi apparatus. The area is called the transitional ER and is considered a boundary for quality control in the case of protein secretion (39). There follows a migration of the lipid body to the cell surface. In the case of the main secretion from the basolateral region, the ER would seem to be the most likely conduit, although we could not observe the ER directly connecting both lipid bodies and the plasma membrane on a thin section for electron microscopy. Because the ER is located near the plasma membrane throughout the cell, it is especially prominent in *B. braunii* (Fig. 6) (33).

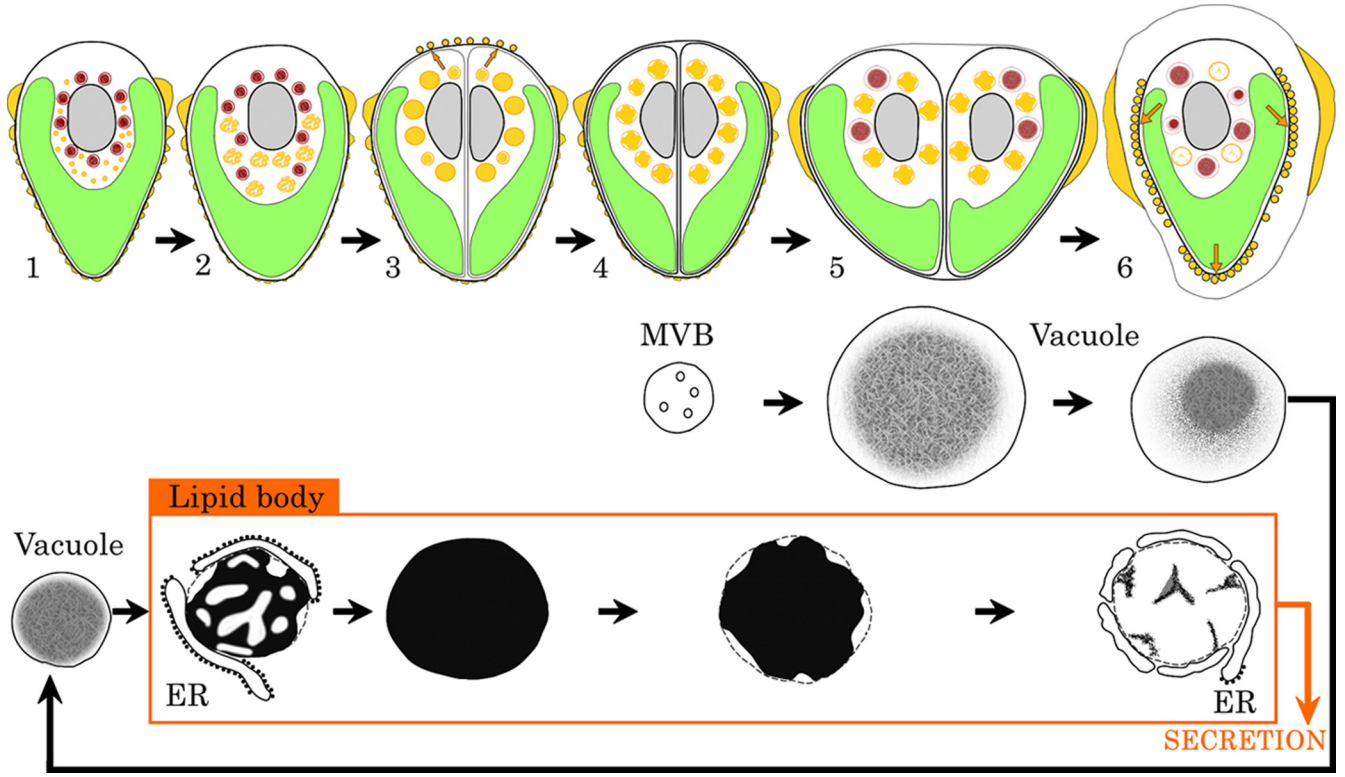

FIG 7 Transformation of lipid bodies and vacuoles during the cell cycle. The top line shows the growth stage of *B. braunii*. Yellow, lipid body in cytoplasm and lipid on the cell surface; red, vacuole; green, chloroplast; gray, nucleus; orange arrow, lipid secretion. The second and third lines show the transformation of lipid bodies and vacuoles. The transformations from the multivesicular body (MVB) to vacuole and from the vacuole to the lipid body were described previously (30).

A radiolabeling experiment by Largeau et al. in 1980 has shown that race A does not secrete cytoplasmic hydrocarbons (9), in contrast to race B, which does secrete cytoplasmic hydrocarbons (15).

The results of the present studies with race A can be explained if the synthesis of extracellular hydrocarbons is not completed in the cytoplasm, but instead precursors are synthesized in the cytoplasm and then secreted to the cell surface. In other words, maturation of hydrocarbons occurs in the extracellular space, as reported by Largeau et al. (9). In this study, we obtained results that support this explanation. There were no special fine structures in the newly accumulated lipid droplets on the cell surface (Fig. 4G and 5C); however, amorphous materials attached to the outer thin layer in the extracellular space usually contained electron-transparent thin layers (Fig. 5C and E and 6E). A definitive answer can be obtained by immunoelectron microscopic detection of the enzyme that catalyzes the final step in the generation of odd-number hydrocarbons.

Accumulation at the cell apex was expected to occur in a short time and in small amounts compared to the basolateral pathway, because the number of lipid bodies did not decrease after secretion. The *trans*-Golgi networks that are located near the cell apex and produce special 400- to 450-nm vesicles only just after septum formation (32) may contribute to the secretion. We will report their role in the future.

ACKNOWLEDGMENTS

An electron micrograph of a thick section was taken with the support of the Research Center for Ultra-High Voltage Electron Microscopy, Osaka University, Japan.

This work was supported by the Japan Science and Technology Agency, CREST.

REFERENCES

1. **Hu Q, Sommerfeld M, Jarvis E, Ghirardi M, Posewitz M, Seibert M, Darzins A.** 2008. Microalgal triacylglycerols as feedstocks for biofuel production: perspectives and advances. Plant J. **54:**621–639.
2. **Rodolfi L, Zittelli GC, Bassi N, Padovani G, Biondi N, Bonini G, Tredici MR.** 2009. Microalgae for oil: strain selection, induction of lipid synthesis and outdoor mass cultivation in a low-cost photobioreactor. Biotechnol. Bioeng. **102:**100–112.
3. **Sheehan J, Dunahay T, Benemann J, Roessler P.** 1998. A look back at the U.S. Department of Energy's Aquatic Species Program: biodiesel from algae. National Renewable Energy Laboratory, Golden, CO. http://www.nrel.gov/biomass/pdfs/24190.pdf.
4. **Maxwell JR, Douglas AG, Eglinton G, McCormick A.** 1968. The botryococcenes—hydrocarbons of novel structure from the alga *Botryococcus braunii* Kützing. Phytochemistry **7:**2157–2171.
5. **Brown AC, Knights BA, Conway E.** 1969. Hydrocarbon content and its relationship to physiological state in the green alga *Botryococcus braunii*. Phytochemistry **8:**543–547.
6. **Berkaloff C, Rousseau B, Couté A, Casadevall E, Metzger P, Chirac C.** 1984. Variability of cell wall structure and hydrocarbon type in different strains of *Botryococcus braunii*. J. Phycol. **20:**377–389.
7. **Casadevall E, Dif D, Largeau C, Gudin C, Chaumont D, Desanti O.** 1985. Studies on batch and continuous cultures of *Botryococcus braunii*: hydrocarbon production in relation to physiological state, cell ultrastructure, and phosphate nutrition. Biotechnol. Bioeng. **27:**286–295.
8. **Largeau C, Casadevall E, Berkaloff C, Dhamelincourt P.** 1980. Sites of accumulation and composition of hydrocarbons in *Botryococcus braunii*. Phytochemistry **19:**1043–1051.
9. **Largeau C, Casadevall E, Berkaloff C.** 1980. The biosynthesis of long-chain hydrocarbons in the green alga *Botryococcus braunii*. Phytochemistry **19:**1081–1085.

10. **Wake LV, Hillen LW.** 1980. Study of a bloom of the oil-rich alga *Botryococcus braunii* in the Darwin River reservoir. Biotechnol. Bioeng. **22:**1637–1656.
11. **Dote Y, Sawayama S, Inoue S, Minowa T, Yokoyama S.** 1994. Recovery of liquid fuel from hydrocarbon-rich microalgae by thermochemical liquefaction. Fuel **73:**1855–1857.
12. **Metzger P, Berkaloff C, Casadevall E, Coute A.** 1985. Alkadiene- and botryococcene-producing races of wild strains of *Botryococcus braunii*. Phytochemistry **24:**2305–2312.
13. **Metzger P, Allard B, Casadevall E, Berkaloff C, Couté A.** 1990. Structure and chemistry of a new chemical race of *Botryococcus brauni* (Chlorophyceae) that produces lycopadiene, a tetraterpenoid hydrocarbon. J. Phycol. **26:**258–266.
14. **Metzger P, Villareal-Rosales E, Casadevall E, Couté A.** 1989. Hydrocarbons, aldehydes and triacylglycerols in some strains of the race A of the green alga *Botryococcus braunii*. Phytochemistry **28:**2349–2353.
15. **Metzger P, David M, Casadevall E.** 1987. Biosynthesis of triterpenoid hydrocarbons in the B-race of the green alga *Botryococcus braunii*. Sites of production and nature of the methylating agent. Phytochemistry **26:**129–134.
16. **Okada S, Murakami M, Yamaguchi K.** 1995. Hydrocarbon composition of newly isolated strains of the green microalga *Botryococcus braunii*. J. Appl. Phycol. **7:**555–559.
17. **Metzger P, Casadevall E.** 1987. Lycopadiene, a tetraterpenoid hydrocarbon from new strains of the green alga *Botryococcus braunii*. Tetrahedron Lett. **28:**3931–3934.
18. **Dennis MW, Kolattukudy PE.** 1991. Alkane biosynthesis by decarbonylation of aldehyde catalyzed by a microsomal preparation from *Botryococcus braunii*. Arch. Biochem. Biophys. **287:**268–275.
19. **Dennis M, Kolattukudy PE.** 1992. A cobalt-porphyrin enzyme converts a fatty aldehyde to a hydrocarbon and CO. Proc. Natl. Acad. Sci. U. S. A. **89:**5306–5310.
20. **Wang X, Kolattukudy PE.** 1995. Solubilization and purification of aldehyde-generating fatty acyl-CoA reductase from green alga *Botryococcus braunii*. FEBS Lett. **370:**15–18.
21. **Okada S, Devarenne TP, Murakami M, Abe H, Chappell J.** 2004. Characterization of botryococcene synthase enzyme activity, a squalene synthase-like activity from the green microalga *Botryococcus braunii*, race B. Arch. Biochem. Biophys. **422:**110–118.
22. **Niehaus TD, Okada S, Devarenne TP, Watt DS, Sviripa V, Chappell J.** 2011. Identification of unique mechanisms for triterpene biosynthesis in *Botryococcus braunii*. Proc. Natl. Acad. Sci. U. S. A. **108:**12260–12265.
23. **Okada S, Devarenne TP, Chappell J.** 2000. Molecular characterization of squalene synthase from the green microalga *Botryococcus braunii*, race B. Arch. Biochem. Biophys. **373:**307–317.
24. **Matsushima D, Jenke-Kodama H, Sato Y, Fukunaga Y, Sumimoto K, Kuzuyama T, Matsunaga S, Okada S.** 2012. The single cellular green microalga *Botryococcus braunii*, race B possesses three distinct 1-deoxy-D-xylulose 5-phosphate synthases. Plant Sci. **185–186:**309–320.
25. **Ioki M, Baba M, Bidadi H, Suzuki I, Shiraiwa Y, Watanabe MM, Nakajima N.** 2012. Modes of hydrocarbon oil biosynthesis revealed by comparative gene expression analysis for race A and race B strains of *Botryococcus braunii*. Biores. Technol. **109:**271–276.
26. **Ioki M, Baba M, Nakajima N, Shiraiwa Y, Watanabe MM.** 2012. Transcriptome analysis of an oil-rich race B strain of *Botryococcus braunii* (BOT-70) by de novo assembly of 5′-end sequences of full-length cDNA clones. Biores. Technol. **109:**277–281.
27. **Molnár I, Lopez D, Wisecaver JH, Devarenne TP, Weiss TL, Pellegrini M, Hackett JD.** 2012. Bio-crude transcriptomics: gene discovery and metabolic network reconstruction for the biosynthesis of the terpenome of the hydrocarbon oil-producing green alga, *Botryococcus braunii* race B (Showa). BMC Genomics **13:**576–603.
28. **Schnepf E, Koch W.** 1978. Über den Feinbau der "Ölalge" Botryococcus braunii Kützing (Chlorococcales). Bot. Jahrb. Syst. Pflanzengesch. Pflanzengeogr. **99:**370–379.
29. **Wolf FR, Cox ER.** 1981. Ultrastructure of active and resting colonies of *Botryococcus braunii* (Chlorophyceae). J. Phycol. **17:**395–405.
30. **Noguchi T.** 1994. Formation and decomposition of vacuoles in *Botryococcus* in relation to the *trans*-Golgi network. Protoplasma **180:**29–38.
31. **Noguchi T, Watanabe H.** 1999. Brefeldin A effects on the *trans*-Golgi network and Golgi bodies in *Botryococcus braunii* are not uniform during the cell cycle. Protoplasma **209:**193–206.
32. **Noguchi T, Kakami F.** 1999. Transformation of *trans*-Golgi network during the cell cycle in a green alga, *Botryococcus braunii*. J. Plant Res. **112:**175–186.
33. **Weiss TL, Roth R, Goodson C, Vitha S, Black I, Azadi P, Rusch J, HoIzenburg A, Devarenne TP, Goodenough U.** 2012. Colony organization in the green alga *Boryococcus braunii* (race B) is specified by a complex extracellular matrix. Eukaryot. Cell **11:**1424–1440.
34. **Weiss TL, Chun HJ, Okada S, Vitha S, Holzenburg A, Laane J, Devarenne TP.** 2010. Raman spectroscopy analysis of botryococcene hydrocarbons from the green microalga *Botryococcus braunii*. J. Biol. Chem. **285:**32458–32466.
35. **Villareal-Rosales E, Metzger P, Casadevall E.** 1992. Ether lipid production in relation to growth in *Botryococcus braunii*. Phytochemistry **31:**3021–3027.
36. **Kunst L, Samuels L.** 2009. Plant cuticles shine: advances in wax biosynthesis and export. Curr. Opin. Plant Biol. **12:**721–727.
37. **Bernard A, Joubès J.** 2013. *Arabidopsis* cuticular waxes: advances in synthesis, export and regulation. Prog. Lipid Res. **52:**110–129.
38. **Tsukada M, Tabata M.** 1984. Intracellular localization and secretion of naphthoquinone pigments in cell cultures of *Lithospermum erythrorhizon*. Planta Med. **50:**338–341.
39. **Farquhar MG, Hauri H.-P.** 1997. Protein sorting and vesicular traffic in the Golgi apparatus, p 63–129. *In* Berger EG, Roth J (ed), The Golgi apparatus. Birkhaüser Verlag, Basel, Switzerland.